

CO EMISSION IN OPTICALLY OBSCURED (TYPE-2) QUASARS AT REDSHIFTS $z \approx 0.1$ - 0.4

M. KRIPS, R. NERI AND P. COX

Institut de Radio Astronomie Millimétrique (IRAM), 300, rue de la Piscine, Domaine Universitaire, 38406 Saint Martin d'Hères, France
Not to appear in Nonlearned J., 45.

ABSTRACT

We present a search for CO emission in a sample of ten type-2 quasar host galaxies with redshifts of $z \approx 0.1$ - 0.4 . We detect CO(J=1-0) line emission with $\geq 5\sigma$ in the velocity integrated intensity maps of five sources. A sixth source shows a tentative detection at the $\sim 4.5\sigma$ level of its CO(J=1-0) line emission. The CO emission of all six sources is spatially coincident with the position at optical, infrared or radio wavelengths. The spectroscopic redshifts derived from the CO(J=1-0) line are very close to the photometric ones for all five detections except for the tentative detection for which we find a much larger discrepancy. We derive gas masses of $\sim (2-16) \times 10^9 M_\odot$ for the CO emission in the six detected sources, while we constrain the gas masses to upper limits of $M_{\text{gas}} \leq 8 \times 10^9 M_\odot$ for the four non-detections. These values are of the order or slightly lower than those derived for type-1 quasars. The line profiles of the CO(J=1-0) emission are rather narrow ($\lesssim 300 \text{ km s}^{-1}$) and single peaked, unveiling no typical signatures for current or recent merger activity, and are comparable to that of type-1 quasars. However, at least one of the observed sources shows a tidal-tail like emission in the optical that is indicative for an on-going or past merging event.

We also address the problem of detecting spurious $\sim 5\sigma$ emission peaks within the field of view.

Subject headings: galaxies: active — galaxies: ISM — infrared radiation — ISM: molecules — quasars: general — radio emission lines

1. INTRODUCTION

Molecular gas is an important diagnostic tracer to study the activity processes in galaxies, whether in form of an accreting super-massive central black hole (AGN) or intense starbursts (SB) or both. It does not only build up the fuel for the activity but also traces essential physical properties of the host galaxy, such as the kinematics, distribution, excitation conditions and chemistry of its gas. As activity occurs in many different types of galaxies and at various levels of intensity and galaxy evolution, a big effort is put into elucidating the physics behind its different occurrences.

Given the elementary importance of molecular gas, numerous studies have been conducted to detect and map its distribution and kinematics in galaxies. Most of them were focussed on sources in the local universe given their easier detectability. However, recent technical improvements make it now possible to probe the higher redshift galaxy population (e.g., Wang et al. 2011a; Riechers et al. 2011, 2009; Tacconi et al. 2010, 2008, 2006; Daddi et al. 2010, 2009; Greve et al. 2005; Neri et al. 2003). This is especially important because most of the active galaxies, such as the ultra-luminous infrared (ULIRGs)/sub-millimeter galaxies and quasars, are found in the high-redshift universe emphasizing the tight correlation of the activity of a galaxy and its evolution. However, it is still poorly understood whether the nature of the activity plays a role for the evolution of a galaxy and how; most current theories assume that both activity types mark a special stage of evolution in a galaxy's life (e.g., Sanders et al. 1988a,b; Hopkins et al. 2006). It is thus surprising that molecular gas has been extensively studied in a large number of (SB-powered) ULIRGs/submillimeter galaxies, while the

(AGN-powered) quasar population still lacks a similarly high number of systematic studies. This lack of information is hence a shortcoming in current theories of galaxy evolution.

While most recent molecular gas studies of quasars at redshifts of $z < 0.5$ concentrate on optically selected sources (type-1 quasars; e.g., Wink et al. 1997; Evans et al. 2001; Scoville et al. 2003; Krips et al. 2005a, 2007; Bertram et al. 2007), evidence has recently been presented that optically obscured (type-2/reddened type-1) quasars may be found at least in equal amounts (at least for $z \lesssim 4$; Reyes et al. 2008; Lacy et al. 2007a; Martínez-Sansigre et al. 2006). Identifying type-2 quasars has been proven to be extremely difficult because of their high obscuration at most wavelengths but success rates have been significantly improved by several groups in the past few years using the less obscured radio, X-ray, and/or Mid-Infrared bands (e.g., Lacy et al. 2007b; Zakamska et al. 2008).

The study of both, type-1 and type-2 quasars, is critical as it challenges the viewing angle and merger-driven unification theories for quasars. While in the viewing-angle unification an edge-on clumpy torus blocks the direct view onto type-2 quasars (Antonucci 1993), the merger-driven unification assumes that type-2 quasars are in an earlier stage of a merging event than type-1 quasars (e.g., Hopkins et al. 2006). The latter scenario finds support by recent observational results: 1.) type-2 quasars are found to have higher median star formation luminosities than type-1 quasars suggesting that type-2 quasar activity goes along with an intensified star formation activity in the host galaxy (e.g., Zakamska et al. 2008) and 2.) the type-2 quasar fraction increases with redshift (e.g., Hasinger 2008; Treister & Urry 2006; LaFranca et al. 2005).

We present here the first systematic search for CO

TABLE 1
SOURCE LIST

Source ^a	Redshift ^b z_{opt}	D_L ^c (Mpc)	Scale (kpc/arcsec)	α_{J2000} ^d (hh:mm:ss.s)	δ_{J2000} ^d (dd:mm:ss.s)	Type ^a
SWIRE2 J021638.21–042250.8	0.304	1565	4.5	02:16:38.20	−04:22:50.8	2
SWIRE2 J021909.60–052512.9	0.099	450	1.7	02:19:09.60	−05:25:12.4	2
SWIRE2 J021939.08–051133.8	0.150	706	2.5	02:19:39.09	−05:11:33.8	2
SWIRE2 J022306.74–050529.1	0.330	1722	4.7	02:23:06.70	−05:05:29.1	2
SWIRE2 J022508.33–053917.7	0.293	1499	4.3	02:25:08.30	−05:39:17.7	2
SDSS J092014.11+453157.3	0.403	2179	5.4	09:20:14.10	+45:31:57.0	2
SDSS J103951.49+643004.2	0.402	2173	5.4	10:39:51.50	+64:30:04.0	2
SSTXFLS J171325.1+590531	0.126	583	2.2	17:13:25.10	+59:05:31.0	2
SSTXFLS J171335.1+584756	0.133	619	2.3	17:13:35.10	+58:47:56.0	1R
SSTXFLS J172123.1+601214	0.325	1691	4.8	17:21:23.10	+60:12:14.0	2

^a taken from Lacy et al. (2007b) and Zakamska et al. (2008).

^b Optical redshifts (spectroscopically determined).

^c Assuming the following cosmology: $\Omega_M=0.27$, $\Omega_\Lambda=0.73$ and $H_0=71 \text{ km s}^{-1} \text{ Mpc}^{-1}$.

^d Positions taken from Simpson et al. (2006) (radio), Lacy et al. (2007b) (optical/IR) or Zakamska et al. (2008) (optical/IR).

^e Type of AGN: 2= optically obscured AGN; 1R=reddened type-1 AGN (type-1= un-obscured AGN).

in optically obscured (type-2) quasars at redshifts $0.09 < z < 0.41$. The general properties of the sources in the sample are summarized in Table 1. The sources were selected based on their $24\mu\text{m}$ -fluxes (MIPS, IRAC) and spectroscopic redshifts from the type-2 quasar studies conducted by Lacy et al. (2007b) and Zakamska et al. (2008). The upper limit for the redshifts was chosen so that the CO(J=1–0) line emission still falls within the 3mm band of the IRAM Plateau de Bure Interferometer (PdBI) receivers. The type-2 quasar sample from Zakamska et al. (2008) originates from the SDSS catalogue and was followed-up with Spitzer. The two samples used in Lacy et al. (2007b) are taken from the SWIRE-(RA=02h) and the Spitzer XFLS fields (RA=17h).

2. OBSERVATIONS

The observations of the CO(J=1–0) emission in a sample of ten type-2 quasars (Table 1) have been conducted at the IRAM PdBI in 2007, 2009 and 2010, using five to six antennas in the most compact configuration (D) with baselines ranging between 15 m and 100 m. A journal of the observations is given in Table 2. We tuned the 3 mm receivers of the PdBI to the redshifted frequency of CO(J=1–0) (115.271 GHz at rest) for each source, using a bandwidth of 1 GHz ($\simeq 3000\text{--}3500 \text{ km/s}$) and a spectral resolution of 2.5 MHz for the observations dated prior to 2010. In 2010, the new wideband correlator WideX was installed at the PdBI so that we had a total of 3.6 GHz of bandwidth at our disposal. Typical system temperatures have been around $\sim 80\text{--}200 \text{ K}$ during the observations. We discarded all data with phase noise exceeding 50 degrees. We calibrated the data using a set of strong sources, including MWC349 for absolute flux calibration. The uncertainty of the absolute flux calibration is estimated to be $\lesssim 10\%$.

3. RESULTS

3.1. Line Emission

We detect CO(J=1–0) emission in five of the ten type-2 quasars and find a tentative detection in a sixth source (see Table 4 and Fig. 1 & 2), resulting in a $\sim 60\%$ detection rate which is similar to previous CO surveys on quasars (e.g., Evans et al. 2001; Scoville et al. 2003;

Bertram et al. 2007). The CO(J=1–0) emission in the remaining four sources remains undetected.

In the course of our observations, we “detected” $\geq 5\sigma$ emission peaks at off-center positions in the field of view of at least four of our ten targets. None of these peaks were found to coincide in position with any of our quasars nor any known galaxy in the NED data base. Statistical considerations (see Appendix) further argue for a spurious nature of these $\sim 5\sigma$ peaks; we dedicate a section on the Appendix to this problem. Otherwise no further consideration is given to these noise peaks in the following.

3.1.1. Detections at the Phase Center

The line emission of five of our ten targets is clearly detected in the line spectrum and the integrated maps. The spatial position of the emission (Fig. 2) as well as the redshift derived from the line centers (Fig. 1) coincide well with the spatial positions from optical/IR/radio observations (Simpson et al. 2006, Table 3) and their photometric redshifts (see Table 1 and 4). The CO redshifts were determined by fitting a Gaussian profile to the line spectrum of each source.

We further find a tentative detection of the CO(J=1–0) emission in a sixth source (see Fig. 1 and 2). A 4.5σ peak is found close to the position of the radio emission of this source. The CO line, however, is significantly shifted bluewards with respect to what is expected from the photometric redshift. The difference is much larger than for any of the other five detected sources. Also, the line profile of the CO(J=1–0) emission is not statistically significant, so that additional observations would be needed to confirm or discard this tentative detection. However, since the 4.5σ peak is within the radio position of this quasar, we think that it is reasonable to assume that this detection is indeed real but we will still treat this source as tentative for the remainder of the discussions.

All six sources exhibit simple line profiles that appear Gaussian in nature, single peaked and narrow. To derive the line intensities, line centers, and line width, we fitted a Gaussian function to all six lines. The results are given in Table 4.

Four out of these six galaxies appear to be unresolved

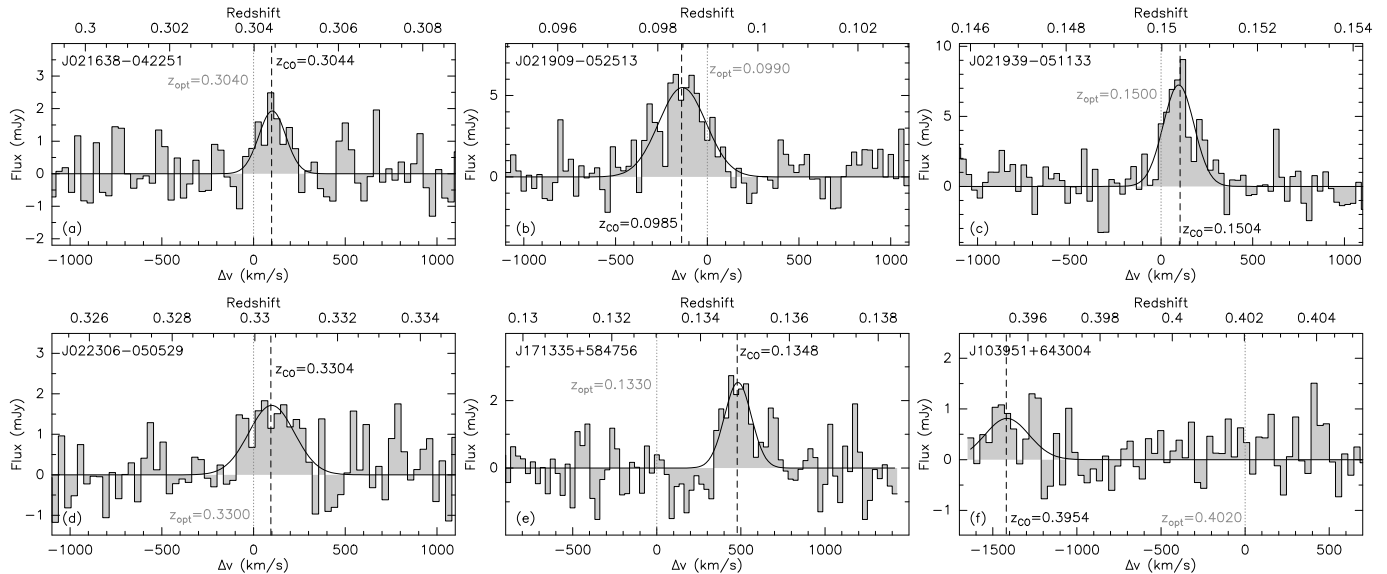


FIG. 1.— Spatially integrated CO(J=1–0) line spectrum of all six CO detections. The zero velocity corresponds to the (spectroscopically derived) optical redshift (*dotted grey lines*). The new redshifts based on the CO(J=1–0) lines are determined from fitting a Gaussian profile to the spectra (*dashed black lines*).

TABLE 2
JOURNAL OF OBSERVATIONS

Source	Observing Date (Year:Month)	Obs. Frequency (GHz)	Integration time ^a (hours)	Synthesized Beam ^b (" × " @ °)
J021638–042250	2009:May,Jun,Jul	88.398	7.4	7.4 × 5.0 @ 153
J021909–052512	2007:Oct,Nov	104.887	1.9	6.9 × 4.8 @ 21
J021939–051133	2007:Sep	100.236	4.0	6.0 × 4.7 @ 161
J022306–050529	2009:May,Jun	86.670	10.3	8.3 × 5.1 @ 148
J022508–053917	2009:Sep,Oct	89.150	5.4	11.1 × 4.6 @ 146
J092014+453157	2009:May,Jun,Aug; 2010:May,Apr	82.206	11.3	6.2 × 4.7 @ 127
J103951+643004	2009:May,Jun; 2010:Apr	82.219	7.6	6.5 × 5.4 @ 129
J171325+590531	2007:Aug	102.372	3.0	5.9 × 3.8 @ 74
J171335+584756	2007:Oct; 2009:Sep	101.740	8.2	5.2 × 3.3 @ 69
J172123+601214	2007:Aug,Sep,Oct	86.997	6.5	7.2 × 5.2 @ 134

^a On-source integration time estimated with respect to 6 antennas and dual polarisation.

^b For natural weighting.

at their detection level and no significant velocity gradient can be identified. Only the CO emission regions of J021909–052513 and J021939–051133 appear to be slightly extended and show a velocity gradient along a North-East to South-West direction (Fig. 3) although the one for J021909–052513 is less pronounced. While the optical i' -image (taken from Simpson et al. 2006) shows a tail-like extension for J021909–052513 indicating a possible interaction with another galaxy, the optical image for J021939–051133 shows a compact galaxy with no signs of disruption. The CO emission in J021909–052513 suggests the presence of molecular gas along the tidal tail of this merger system. Fitting a Gaussian to the uv-data results in a size estimate of $2 \pm 1''$ (~ 5 kpc), i.e., very centralised molecular gas. However, at the angular resolution and sensitivity of our observations, we cannot exclude that part of the more extended diffuse gas might have been resolved out.

3.1.2. Non-detections

Although we cannot entirely rule out this possibility, we doubt that the four non-detections are due

to uncertainties in the optical spectroscopic redshifts. Hainline et al. (2004) present a comparison between optical and CO redshifts in high-redshift sources. The authors find, excluding a few outliers, a difference of $|\Delta z_{\max}| = |z_{\text{opt}} - z_{\text{CO}}| \lesssim 0.008$, which corresponds to a velocity shift of $\sim \pm(1500-2000)$ km s⁻¹ at 3.5 mm in the redshift range $z=0.2-0.5$. A similar deviation of ~ 0.008 is seen when adding the CO detections at high- z since 2005 (e.g., Greve et al. 2005; Coppin et al. 2008). Interestingly, the outliers which show $0.008 < \Delta z \lesssim 0.05$ all lie at redshift $z \geq 2.5$. Therefore, the large bandwidth of 3000 km s⁻¹ should be sufficiently large to take out uncertainties in the optical redshift for the sources presented in this paper. However, it has to be pointed out that for the determination of the difference Δz only sources with *detected* CO emission were considered. The actual deviation Δz could be hence larger than assumed here. Only larger bandwidth (≥ 4 GHz) and higher sensitivity (going down to $M_{\text{gas}} \lesssim 10^8 M_{\odot}$ where $M_{\text{gas}} = M(\text{H}_2 + \text{He})$ is the total gas mass) observations will allow us to reliably eliminate all uncertainties from optical redshifts for the detection of CO emission in higher- z

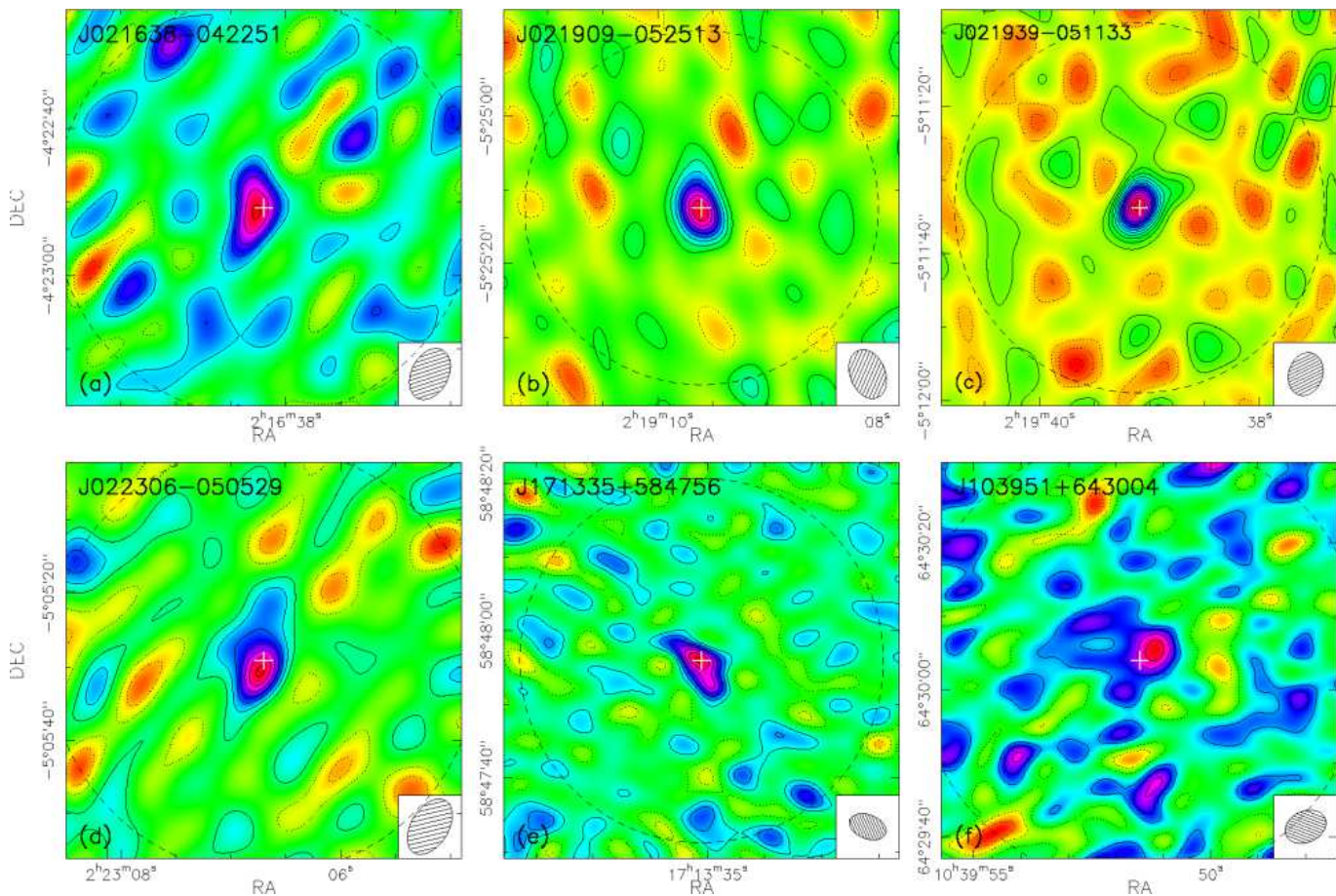


FIG. 2.— Velocity integrated CO($J=1-0$) line emission maps of the six detected type-2 quasar host galaxies. The large dashed circles indicate the field of view for each target. The synthesized beams are shown in the lower right corner of each map. Negative contours (dotted) correspond to $-3, -2, -1\sigma$, and positive contours (solid) start at 1σ in steps of 1σ with the following noise levels for each map: (a) $1\sigma=0.05$ Jy beam $^{-1}$ km s $^{-1}$ ($\Delta v_{\text{int}}\simeq 220$ km s $^{-1}$); (b) $1\sigma=0.58$ Jy beam $^{-1}$ km s $^{-1}$ ($\Delta v_{\text{int}}\simeq 490$ km s $^{-1}$); (c) $1\sigma=0.39$ Jy beam $^{-1}$ km s $^{-1}$ ($\Delta v_{\text{int}}\simeq 330$ km s $^{-1}$); (d) $1\sigma=0.08$ Jy beam $^{-1}$ km s $^{-1}$ ($\Delta v_{\text{int}}\simeq 400$ km s $^{-1}$); (e) $1\sigma=0.08$ Jy beam $^{-1}$ km s $^{-1}$ ($\Delta v_{\text{int}}\simeq 350$ km s $^{-1}$); (f) $1\sigma=0.07$ Jy beam $^{-1}$ km s $^{-1}$ ($\Delta v_{\text{int}}\simeq 420$ km s $^{-1}$)

sources.

3.2. Continuum Emission

Continuum emission at 3 mm has not been found in any of the ten sources. The 3σ upper limits derived for the 3 mm continuum fluxes (Table 4) are similar or slightly lower than the 1.4 GHz flux densities (Table 3) excluding a flat radio spectrum in these sources and pointing rather towards a steep radio spectrum. A steep radio spectrum is generally associated with non-thermal emission which is typically found in this galaxy population. However, extrapolating the 1.4 GHz flux densities (Table 3) with a spectral index of -1 (i.e., $f_\nu \propto \nu^{-1}$) infers flux densities at 3 mm that are smaller by an order of magnitude than our 3 sigma upper limits. We also stacked the continuum maps from all ten targets with no significant detection in the stacked image, i.e., the emission peak in the center remains at $\lesssim 3\sigma=0.09$ mJy. Thus, no definite conclusion can be drawn on the nature of the 3 mm continuum emission in our sources.

4. DISCUSSION AND CONCLUSIONS

4.1. Molecular Gas Masses

Using the standard Galactic conversion factor for the $M_{\text{gas-to-L}'_{\text{CO}}}$ ratio of $X_{\text{CO}}=4.8$ M $_{\odot}$ (K km s $^{-1}$ pc 2) $^{-1}$

(e.g., Solomon & Barret 1991), we find a range of the total gas mass of $M_{\text{gas}}\simeq(2-16)\times 10^9 M_{\odot}$ for all five detected sources (plus the one tentatively detected) and 3σ upper limits for the four non-detections of $M_{\text{gas}}\lesssim(2-8)\times 10^9 M_{\odot}$ (Table 4). However, the standard Galactic conversion factor X_{CO} is known to over-estimate the total gas mass in the ULIRG/submillimeter population by more than a factor of 5 (e.g., Downes & Solomon 1998) and seems to be also highly dependent on the physical properties (e.g., metallicity; Bell et al. 2007a,b). Bell et al. (2007b) find indications for a lower X_{CO} in AGN dominated galaxies in the local universe as well (e.g., M51). If this were also true for higher- z quasars, the gas masses for the sources in this paper would reduce to values below $3\times 10^9 M_{\odot}$.

4.2. Dynamical Masses

Assuming a radius of the emission equal or lower than half the synthesized beam (i.e., $\sim 3-5''\simeq 5-15$ kpc) and taking the full width at half maximum (FWHM) of the line profiles determined for the six detected sources, the dynamical masses amount to $\sim(10^{10}-10^{12})M_{\odot}\times\sin^{-2}i$ with i being the disk inclination angle. These dynamical masses easily account for the obtained total gas mass within the assumed radius of 5-15 kpc ($\simeq 10\%$ of the stellar amount in the entire galaxy, which is a few times

TABLE 3
BOLOMETRIC (RADIO, IR, X-RAY) PROPERTIES OF THE OBSERVED SOURCES

Source	$S_{160\mu\text{m}}^a$ (mJy)	$S_{70\mu\text{m}}^a$ (mJy)	$S_{24\mu\text{m}}^a$ (mJy)	$S_{8\mu\text{m}}^a$ (mJy)	L_{FIR}^b ($10^{10}L_{\odot}$)	L_{MIR}^b ($10^{10}L_{\odot}$)	L_{IR}^b ($10^{10}L_{\odot}$)	$S_{1.4\text{GHz}}^c$ (mJy)	$S_{0.2-12\text{keV}}^d$ ($10^{-14}\text{ergs}^{-1}\text{cm}^{-2}$)
J021638-042251	...	27	14.6	2.7	>8	~23	>32
J021909-052513	152	130	25.6	3.1	~6	~3	~9	1.36±0.02	2.6
J021939-051133	...	70	32.9	8.5	~4	~11	>15	1.24±0.06	5.3
J022306-050529	15.7	1.5	...	~30	>30	...	0.95
J022508-053917	...	32	9.6	2.6	>9	~14	>23
J092014+453157	~8	...	44
J103951+643004	~13	4.3±0.5	70
J171325+590531	9.5	1.19	...	~2	>2	0.16±0.03	...
J171335+584756	146	97	23.7	...	~9	~6	~15	3.4±0.2	...
J172123+601214	13.3	3.71	~4 ^d	~25	~29	0.26±0.04	...

^a taken from Lacy et al. (2004), Lacy et al. (2007b), Frayer et al. (2006) and/or from the SWIRE catalogue available at http://swire.ipac.caltech.edu/swire/astronomers/data_access.html.

^b determined based on $L_{\text{FIR}} = \zeta_2(z)\nu L_{\nu}(70\mu\text{m}) + \zeta_3(z)\nu L_{\nu}(160\mu\text{m})$, $L_{\text{MIR}} = \zeta_1(z)\nu L_{\nu}(25\mu\text{m})$, and $L_{\text{IR}} = L_{\text{FIR}} + L_{\text{MIR}}$ from Dale & Helou (2002); with $\zeta_1(z \approx 0.1) \approx 1.75$, $\zeta_1(z \approx 0.3) \approx 2.2$, $\zeta_2(z \approx 0.1) \approx \zeta_2(z \approx 0.3) \approx 0.82$, $\zeta_3(z \approx 0.1) \approx \zeta_3(z \approx 0.3) \approx 1.347$. The IR luminosities for J092014+453157 and J103951+643004 were taken from Zakamska et al. (2008).

^c References: J17-sources: Condon et al. (2003), J02-sources: Simpson et al. (2006), J103951+643004 from Condon et al. (1998).

^d from Lacy et al. (2007b) and Zakamska et al. (2008).

TABLE 4
OBSERVATIONAL RESULTS

Source	RMS ^a (mJy)	f_{cont}^b (mJy)	$f_{\text{CO}}^{c,d}$ (mJy)	Δv_{FWHM}^e (km s ⁻¹)	v_0^f (km s ⁻¹)	z_{CO}^g	S_{CO}^d (Jy km s ⁻¹)	L'_{CO}^d (K km s ⁻¹ pc ²)	$M_{\text{gas}}^{d,h}$ ($10^9 M_{\odot}$)
DETECTIONS									
J021638-042251	0.8	≤0.3	2.0±0.4	170±40	+102±17	0.3044±0.0002	0.5±0.1	(23±5)×10 ⁸	11±2
J021909-052513	1.4	≤0.6	5.6±0.6	300±40	-135±16	0.0985±0.0006	1.5±0.3	(7±1)×10 ⁸	3.2±0.6
J021939-051133	1.6	≤0.5	7.3±0.7	200±30	+100±10	0.1504±0.0002	1.6±0.2	(17±2)×10 ⁸	8±1
J022306-050529	0.7	≤0.2	1.7±0.3	290±60	+98±27	0.3304±0.0004	0.6±0.1	(33±5)×10 ⁸	16±3
J171335+584756	0.8	≤0.3	2.5±0.4	190±30	+480±10	0.1348±0.0003	0.45±0.08	(5±1)×10 ⁸	2.4±0.4
TENTATIVE DETECTIONS									
J103951+643004	0.6	≤0.2	0.81±0.26	310±120	-1415±50	0.3954±0.0006	0.25±0.06	(21±5)×10 ⁸	10±2
NON-DETECTIONS									
J022508-053917	0.3	≤0.3	≤0.9	≤0.3 ⁱ	≤13×10 ⁸	≤6
J092014+453157	0.2	≤0.2	≤0.6	≤0.2 ⁱ	≤17×10 ⁸	≤8
J171325+590531	0.5	≤0.5	≤1.5	≤0.4 ⁱ	≤3×10 ⁸	≤2
J172123+601214	0.2	≤0.2	≤0.6	≤0.2 ⁱ	≤11×10 ⁸	≤5

^a RMS noise determined from channels with 10 MHz spectral resolution ($\approx 28\text{ km s}^{-1}$) for the CO detections and with 105 MHz spectral resolution ($\approx 300\text{ km s}^{-1}$) for the CO non-detections.

^b 3σ -upper limits for the continuum flux averaged over the line-free channels for each source.

^c Peak line fluxes for the detections and 3σ -upper limits for the non-detections.

^d Errors are of pure statistical nature and do not account for uncertainties from the absolute flux calibration. The latter is estimated to be at a conservative level of $\sim 10\%$. The integrated flux densities have been determined assuming that the continuum emission in these sources is negligible at the given noise level (see also text).

^e Δv_{FWHM} = Full Width at Half Maximum of the line. Determined from CO line profile by fitting a Gaussian to the data.

^f Systemic velocity; zero velocity corresponding to the optical redshifts of the sources.

^g Redshift determined from the central velocity of the CO(J=1-0) line.

^h The standard galactic M_{gas} -to- L'_{CO} conversion factor of $X_{\text{CO}} = 4.8 M_{\odot} (\text{K km s}^{-1} \text{ pc}^2)^{-1}$ has been assumed.

ⁱ Assuming a Δv_{FWHM} of $\sim 260\text{ km s}^{-1}$ corresponding to the average of the FWHM of the detected sources.

$10^{12}M_{\odot}$) and leave enough room for additional material, such as the super-massive central black hole (up to $\sim 10^{10}M_{\odot}$ in the most extreme cases) and the stellar content (up to a few times $10^{11}M_{\odot}$).

4.3. CO versus IR Luminosities

Comparing the CO-luminosities for the detected sources and the upper limits for the undetected ones with those of type-1 quasars taken from the literature (e.g., Evans et al. 2001; Scoville et al. 2003; Bertram et al. 2007), we find that they fall within the same area in

the L'_{CO} - L_{IR} diagram (Fig. 4). However, it has to be noted that most of the IR luminosities assumed for the type-2(1R) quasars must probably be regarded as lower limits (see Table 3). Several of our type-2 quasars have no measured/detected FIR fluxes. Also, obscuration through dust might significantly reduce the emission at MIR wavelengths. However, based on comparison with other dust enshrouded quasars, the IR-luminosities can be larger by up to an order of magnitude than the MIR-luminosities reducing hence the significance of the MIR to the total IR-luminosities.

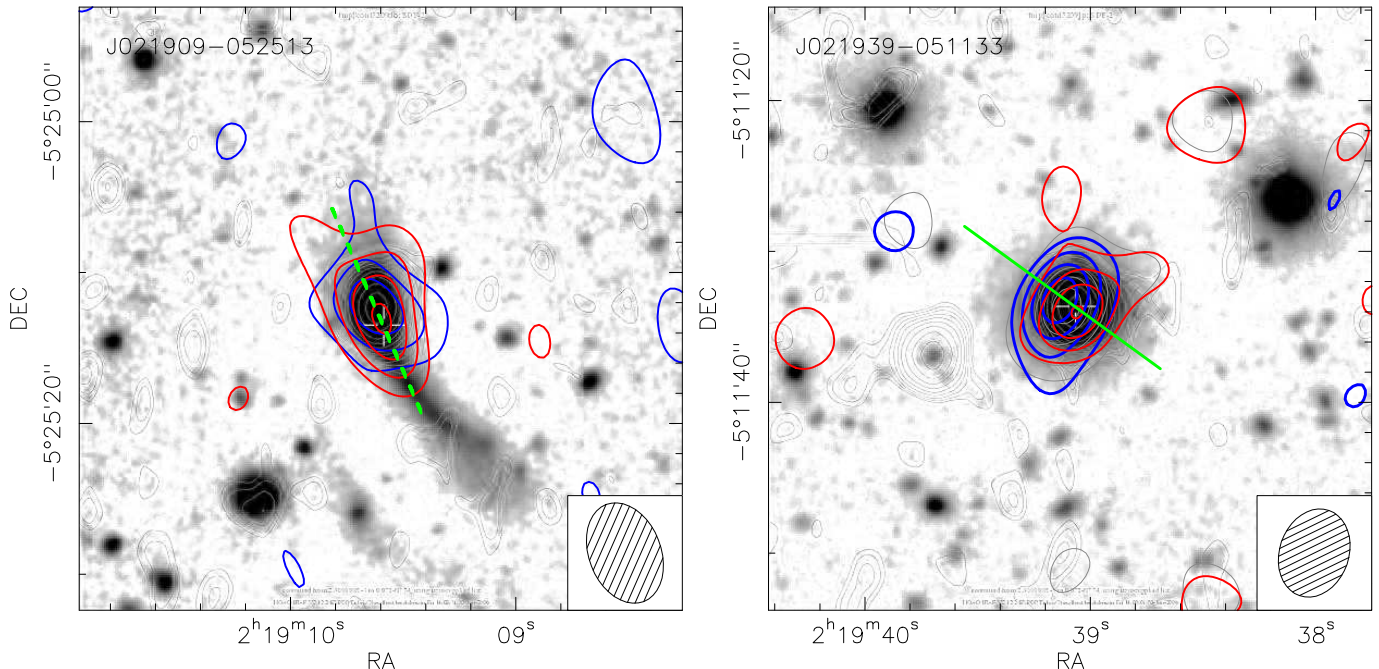


FIG. 3.— Blue- and redshifted CO(J=1–0) line emission (*contours*) of J021909–052513 (*left panel*) and J021939–051133 (*right panel*) overlaid to the Subaru/Suprime-Cam *i'* image (*grey scale*) and the radio emission (*faint grey contours*) taken from Simpson et al. (2006). The velocity gradient is identified with a green line; the green line is dashed for J021909–052513 because a velocity gradient is much more difficult to identify than for J021939–051133. Contours start at 2σ and go in steps of 2σ .

Taking all published CO detections in quasars into account and excluding the upper and lower limits for some of the CO and IR luminosities, we find a linear correlation between the CO and IR luminosities of 0.70 ± 0.03 dex (Fig. 4). When considering the upper limits for the CO luminosities and, separately, the lower limits for the IR luminosities, we obtain a very similar slope of 0.69 ± 0.03 dex based on the analytical method described in Feigelson & Nelson (1985). This is in good agreement with results found for ULIRGs and nearby active galaxies (e.g., Gao & Solomon 2004; Narayanan et al. 2008a). However, some of the upper limits of the CO observations fall significantly below the correlation but it is unclear whether this is due to a breakdown in the correlation, to uncertainties in the optical redshift and/or the significant contribution of the AGN to the (M)IR-luminosities that might even dominate over that from star-formation (e.g., Lacy et al. 2007b; Brand et al. 2006). Besides obscuration effects, the latter represents an important factor in determining “accurate” (i.e., purely star-formation related) IR-luminosities in particular for type-2 quasars. However, the significance of the AGN contribution to the energy output remains also strongly debated for ULIRGs (e.g., Franceschini et al. 2003; Imanishi et al. 2007) so that the importance of the AGN influence on the correlation between CO and IR-luminosities is hard to quantify. On the other hand, the similarity of this correlation between ULIRGs and quasars may indicate that either the AGN contribution influences the correlation in the same way for these sources (such as adding an offset in a systematic way) or is even a fundamental part of the correlation. A detailed entangling of the different part of the correlation is certainly necessary to further our understanding of this very fundamental correlation.

Alternatively, the slope of the $L'_{\text{CO}}-L_{\text{IR}}$ correla-

tion could also vary for different galaxies (as discussed by Gao & Solomon 2004; Bertram et al. 2007). Bertram et al. (2007) suggests a scenario in which geometrical effects naturally lead to a change in slope: galaxies with highly centralised and confined molecular gas (such as ULIRGs) have a larger surface filling factor and thus a steeper slope whilst ‘normal’ weakly interacting/active galaxies show more extended molecular gas resulting in a milder slope. The similarity of the slope between ULIRGs and quasars might hence be an indication that merger events are also important for the quasar population. However, more observations and studies of the distribution of CO in quasars, and active galaxies in general, have to be undertaken to validate this interpretation.

4.4. CO Luminosities versus redshift

Plotting the CO luminosities of the quasars detected in CO against their redshifts (right panel of Fig. 4), suggests that, despite similar IR luminosities, type-2 quasars have lower CO luminosities, and hence a lower amount of molecular gas at comparable stages of evolution than type-1 quasars, i.e., similar redshifts; this impression is mainly given when looking at redshifts between 0.08 and 0.2 (above redshifts of 0.2 and below redshifts of 1.0 no CO detection for type-1 quasars has yet been reported). When applying the statistical analysis from Feigelson & Nelson (1985) that includes the upper limits (see also previous Section) we do find marginally different mean values for the CO luminosities in type-1 quasars of $\langle L'_{\text{CO}} \rangle = (13 \pm 4) \times 10^8$ (K km/s pc²) and those in type-2 quasars of $\langle L'_{\text{CO}} \rangle = (8 \pm 3) \times 10^8$ (K km/s pc²) for redshifts between 0.08 and 0.2; for the entire type-1 and type-2 quasar samples we find almost the same mean values of $\langle L'_{\text{CO}} \rangle = (12 \pm 3) \times 10^8$ (K km/s pc²). However, not only do the mean values agree within the errors, a logrank analysis (Feigelson & Nelson 1985) also shows

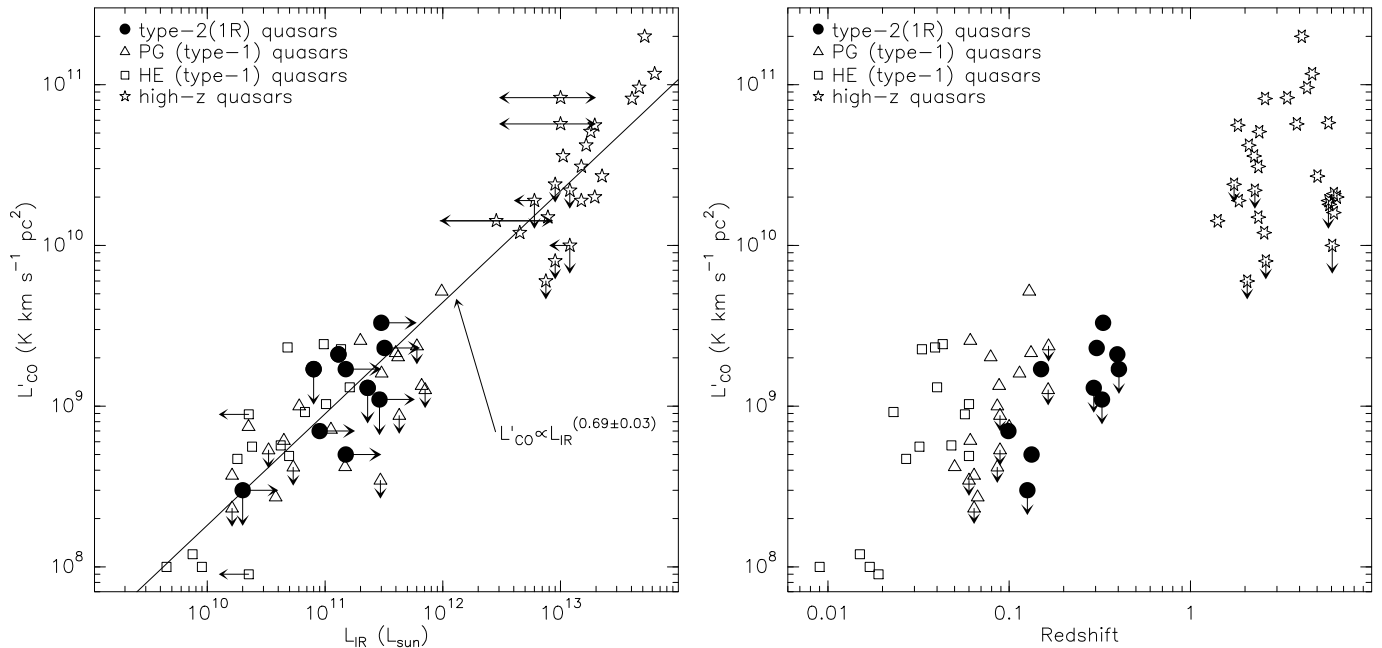


FIG. 4.— CO versus IR luminosity plot (*left*) and CO luminosity versus redshift plot (*right*) of quasars with CO measurements taken from this paper (filled black circles) and the literature (open symbols). The solid black curve (*left*) is a linear fit to the data. Given their high dust obscuration, the IR-luminosities of the type-2(1R) quasars can only be regarded as lower limits. Upper and lower limits are marked with arrows. For some of the high-redshift sources ($z \geq 1$), only FIR luminosities were available, so we assume $L_{\text{IR}} = 1.5 \times L_{\text{FIR}}$ based on a L_{FIR} -to- L_{IR} comparison done by Pott et al. (2006); please note that some quasars can show a ratio larger by a factor of 2-4 because of the contribution of the AGN to the MIR luminosity. However, increasing the ratio to 4 does not significantly change the slope of the correlation and is taken into account in the error of the fit. The references for the literature data are as follows: PG quasars – Evans et al. (2001); Scoville et al. (2003); HE quasars – Bertram et al. (2007); high- z quasars – Wang et al. (2011a,b); Polletta et al. (2011); Coppin et al. (2008); Aravena et al. (2008); Maiolino et al. (2007); Krips et al. (2005b); Walter et al. (2004); Carilli et al. (2002); Cox et al. (2002).

that both samples are similar at a 50% significance level. Therefore we can neither rule out that both samples exhibit similar CO luminosities nor can we support it with the current samples.

Even if the CO luminosities were proven to be lower in type-2 than type-1 sources this would be at odds with both unification theories. The nature of the viewing-angle unification theory suggests that no statistically relevant differences should exist between CO luminosities of type-1 and type-2 quasars. On the other hand, if the merger-driven unification were to hold true, higher CO luminosities (i.e., higher molecular gas masses) would be expected for type-2 quasars.

Thus, different explanations must be considered. One would be the low number statistics. An alternative reason could be the different selection criteria used for the CO surveys of the type-1 and type-2 quasars. It seems that the type-1 quasars were chosen based on their bright IR luminosities while this wasn't a criterium for the type-2 sources. The type-1 quasar sample might hence be biased toward gas rich sources. Also, we cannot exclude resolution effects and hence an underestimation of the CO luminosities in our interferometric study. However, the interferometric observations carried out by Evans et al. (2001) and Scoville et al. (2003) probably suffered from similar problems given the similar redshift ranges of the targets and hence similar spatial scales. Only larger samples will help to settle the question whether the CO luminosities are different for the two quasar populations.

4.5. Linewidth of CO Emission

In case of a lack of sufficient angular resolution, the linewidth of molecular lines can be a first-order merger-activity indicator for galaxies, i.e., the larger the linewidth the more likely a galaxy might be interacting or merging with another galaxy (e.g., Arp 220; see also Greve et al. 2005); however, the contrary is not necessarily true. Comparing hence the linewidths of our type-2 quasars with that of ULIRGs and high- z galaxies (Fig. 5), for which a high percentage is assumed to be in a merger stage, shows indeed that the distribution of the linewidth peaks at higher values for the ULIRG/high-redshift galaxy population than for the nearby type-2 quasars. Also, the ULIRG/high-redshift galaxy population exhibits some very large linewidths with values exceeding 500 km/s as opposed to the type-2 quasars for which all measured linewidths stay well below 400 km/s. No clear difference though can be identified between the type-2 and type-1 quasars; the same is also true for the more local type-1 and type-2 Seyfert galaxies. Both quasars and Seyferts reveal a similar distribution of their linewidths. A significant difference in the distribution of the linewidth between the type-1 and type-2 quasars could favor a merger-driven unification theory; the broadest linewidths should occur for pre-coalescent mergers for which the gas disks of the merging galaxies have not yet met (e.g., Iono et al. 2009).

Even in the viewing-angle unification, one might expect a difference between the linewidths for type-1 and type-2 quasars under certain assumptions. Let us assume that the molecular gas is mostly located in a disk in these quasars and that this (large-scale) disk exhibits a similar inclination to the putative (small-scale) torus. If that were true, the CO emission would be mostly seen

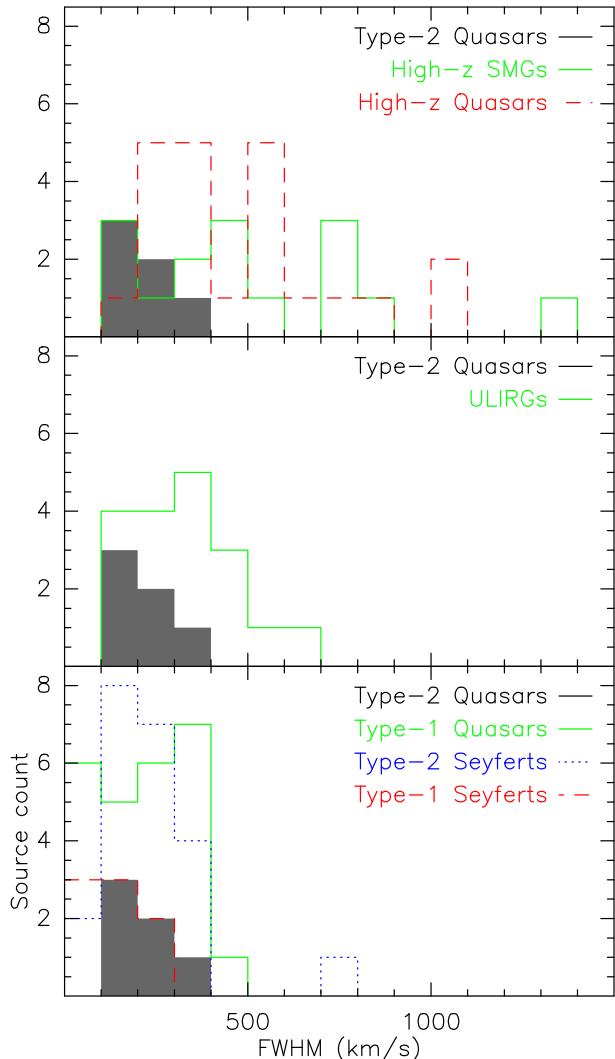


FIG. 5.— A comparison of the measured CO linewidth of the six detected type-2 quasars to other active galaxies in the local and high-redshift universe; the histograms were derived such as that $\text{FWHM}_{\min} < \text{FWHM} \leq \text{FWHM}_{\max}$. The FWHM for the ULIRGs and high-redshift galaxies are taken from references given in Fig. 4 and Iono et al. (2009), for the nearby Seyfert galaxies and type-1 quasars from Barvainis et al. (1989); Alloin et al. (1992); Vila-Vilaro et al. (1998); Sakamoto et al. (1999); Evans et al. (2001); Scoville et al. (2003); Krips et al. (2005a); Bertram et al. (2007). *Note of caution: not corrected for inclination; the CO for the high-z sources is mostly observed at $J_{\text{upper}} > 1$ so that their FWHM might be even higher.*

edge-on in type-2 and face-on in type-1 quasars. In turn this means that the CO linewidth would generally be larger for type-2 than for type-1 quasars. However, overall the linewidths are not expected to exceed values of 500 km s^{-1} as found in mergers. Therefore, a distinction

to the merger unification should still be possible. On the other hand, the assumptions made above may not be valid. If a merging event is indeed taking place in these systems, the molecular gas might be located in a severely disrupted disk for which an inclination would be difficult to derive. Also, even if located in a well defined (large scale) disk, its inclination does not have to be the same as that of a small scale torus (see for instance the discussion for M51 and NGC 1068 in: Matsushita et al. 2007; Krips et al. 2011).

However, one has to keep in mind that there are a few caveats to be considered for this comparison. First, the size of the sample suffers from small number statistics. Second, no correction has been done for disk inclination effects, but, since this is true for all galaxy populations used here, the effects are assumed to be on average the same for all and to cancel each other out. Third, the CO lines for the high-redshift galaxy population have been detected in higher rotational transitions which can underestimate the actual linewidth as they tend to trace the warmer and more compact molecular gas. Fourth, also the possible presence of gas outflows is to be considered a linewidth broadening factor (e.g., Narayanan et al. 2006, 2008b,c; Greve & Sommer-Larsen 2008; Feruglio et al. 2010).

5. SUMMARY

We detected the CO($J=1-0$) line emission in five out of a sample of ten type-2 quasars. We further report on the tentative detection of the CO($J=1-0$) line emission in a sixth source. The estimated molecular gas masses are rather moderate with values not exceeding $2 \times 10^{10} M_{\odot}$. All detections nicely follow the L'_{CO} -to- L_{IR} correlation for quasars. The CO luminosities derived for the six detections and the upper limits for the remaining four type-2 quasars seem to lie slightly below that of previously detected type-1 quasars for similar redshifts. However, given the low number statistics of the current samples this difference is not found to be at a statistically significant level and might simply be due to a selection bias. The rather simple CO($J=1-0$) line profiles and moderate CO luminosities do not seem to support a recent or current merger activity in these sources; however, at least in the case of one source, J021909–052513, the presence of a tidal tail in the optical images is strongly suggestive of a recent or on-going merger event. The data discussed in this paper do not allow to favor either the merger-driven or the viewing angle unification models. Higher number statistics are mandatory to support one or the other scenario.

APPENDIX

DETECTIONS OF $\sim 5\sigma$ PEAKS AT OFF-CENTER POSITIONS

The CO detections and non-detections for the ten sources were determined by running an automated procedure on the calibrated data cubes in both the uv- and the (dirty) image plane. This procedure generates integrated maps for all consecutive channel combinations, i.e., for a 100-channel data cube the code integrates channel number 1 to 2, 1 to 3, ..., 1 to 100, 2 to 3, 2 to 4, 2 to 100, until it reaches 99 to 100. It then searches for the emission maximum in each of the integrated maps and derives the absolute maximum of those individual maxima. This provides a robust and unbiased approach in the search for line emission in large spectral data cubes. With this method several $\geq 5\sigma$ line emission peaks were observed in addition to the detections and non-detections at the center of the arrays field of view.

The uncertainties of the optical/IR positions of the type-2 quasars are smaller than $1''$. This is much smaller than

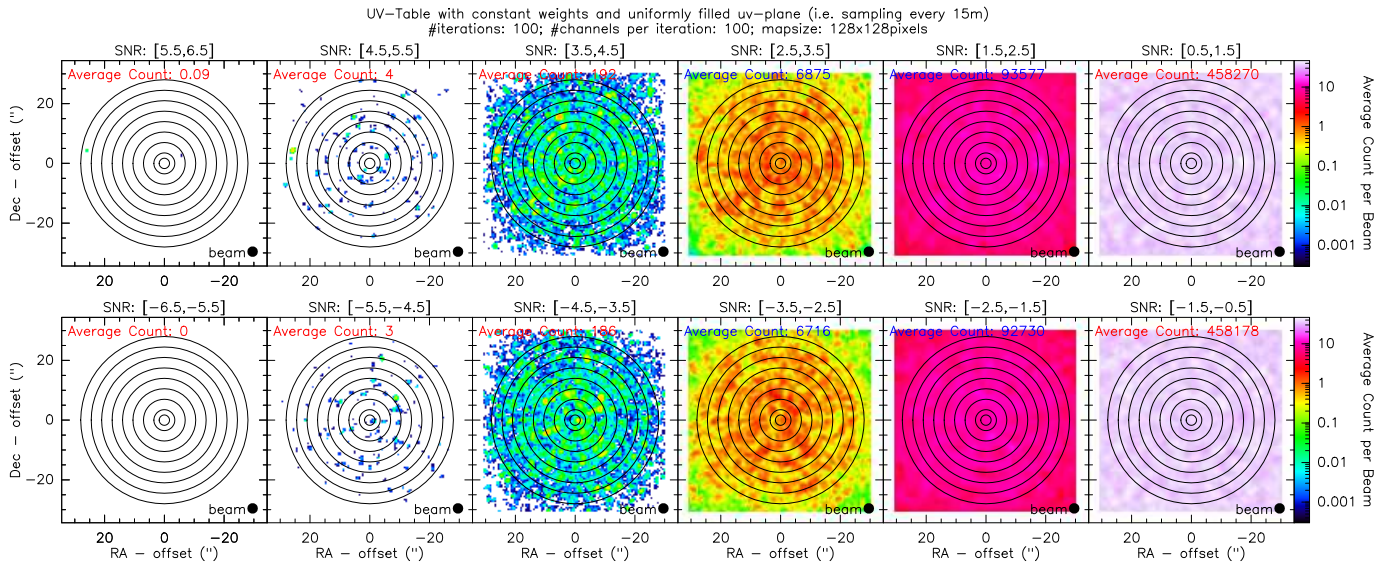


FIG. 6.— Statistical analysis of the Gaussian noise peak distribution for a uniformly filled uv-coverage with one visibility of constant weight every 15m. 100 independent simulations for a 100-channel data cube have been run (for an observing frequency of ~ 100 GHz in D configuration of the PdBI). The maps show the average number count per pixel for each peak intensity normalised by the beamsize within a certain σ -range. The sum of the total number of peaks per map divided by the number of repetitions and normalised by the beamsize is given in the upper left corner of each map. The top panels show the positive peaks, the bottom panels the negative ones. The circles indicate radii starting at $0.5 \times \theta_s$, θ_s and then increasing in steps of θ_s ($\theta_s = 3.5''$). The synthesised beam θ_s is shown in the lower right corner.

the difference between the actually targeted type-2 quasars and the detected emission peaks which were found to be off by more than $\sim 5''$ from the quasar position ($\geq 2 \cdot 10 \theta_s$). A positional search close to the peaks using NED did not show any other galaxies that could be associated with these peaks raising doubts about the reliability of these detections.

Although a $\geq 5\sigma$ peak in the velocity integrated intensity map is generally assumed to mark a reliable detection limit for line emission with the IRAM PdBI, even for off center positions, the significant increase in spectral bandwidth might necessitate a refinement of this detection limit based on statistical considerations. The probability of finding several consecutive $2\text{--}3\sigma$ noise peaks in adjacent spectral channels at any position within ($1.5 \times$) the primary beam increases with the spectral bandwidth and ultimately leads to spurious detections. In order to assess the probability of spurious detections, we conducted a statistical analysis of the data based on an ideal noise distribution as a starting point. Ideal in this context stands for a uniformly filled uv-plane (i.e., one visibility with a constant weight every 15m in either direction up to the maximum D-configuration baseline of 100m used in the actual observations) and a Gaussian noise distribution. We used 100 channels per simulated data cube with 128×128 pixels per channel map. We ran the aforementioned “peak-finder” procedure and repeated this 100 times, every time with a re-computed noise distribution. The results are shown in Fig. 6. A peak-count map is shown for different levels of detection in units of σ , i.e., as multiples of the rms noise (starting from 0.5σ up to 6.5σ peaks). The upper panel shows the average counts of positive peaks per pixel normalised to the beamsize while the lower panel that of the negative ones. The absolute average count that is derived from the total counts per map divided by the number of iterations (100) and normalised by the beamsize ($\sim 30 \text{ pixel}^2$ per beam) is plotted in each SNR range map. The circles indicate different radii, starting at $r = \theta_s/2$, θ_s and increasing then in steps of θ_s ; in our example the synthesized beam has a size of $\theta_s = 3.5''$ (for an observing frequency of ~ 100 GHz in D configuration).

Even in the ideal case of uncorrelated noise, constant visibility weights and even sampling of the uv-plane, we obtain, on average, at least one $\sim 5\sigma$ peak anywhere in ($1.5 \times$) the primary beam. Even the probability to find a peak with $> 5.5\sigma$ is non-zero and lies at the $\sim 9\%$ level. In other words, for a CO line survey of 10 sources this hence means that one spurious $\geq 5.5\sigma$ peak will appear within the field of view of at least one of the ten sources. Furthermore, close to the center of the field of view, i.e., within a radius equal to the size of θ_s , the probability to find a $\sim 5\sigma$ peak is estimated to be at the $\sim 5\%$ significance level. Decreasing this circle however further below a radius of $\sim 1.75''$ ($\equiv 5$ times the positional uncertainty σ_p for a synthesized beam of $\theta_s = 3.5''$ and a signal to noise ratio of $\text{SNR} = 5\sigma$ assuming $\sigma_p = \theta_s / (2\text{SNR})$), the probability drops to almost zero to detect a noise peak with $\geq 4.5\sigma$, giving statistical support for the tentative detection of the CO(J=1–0) emission in J103951+643004.

Obviously, an uneven sampling of the uv-plane, systematic calibration uncertainties, and correlated noise between adjacent channel maps and pixels is likely to increase the number of $> 4.5\sigma$ peaks in the field of view. Spurious detections will certainly challenge future detection surveys as bandwidths will steadily increase in the coming years, especially in the context of a blind survey for line emission from galaxies at high redshift. Based on these statistics, we repeated the observations for those sources for which we found $\geq 5\sigma$ off-center peaks within the field of view. None of these peaks could be confirmed to be real.

REFERENCES

- Alloin, D.; Barvainis, R.; Gordon, M. A.; Antonucci, R. R. J., 1992, A&A, 265, 429
 Aravena, M.; et al., 2008, A&A, 491, 173

- Barvainis, R.; Alloin, D.; Antonucci, R., 1989, *ApJ*, 337, L69
- Bell, T. A.; Roueff, E., Viti, S., Williams, D. A., 2007a, *MNRAS*, 371, 1865
- Bell, T. A.; Roueff, E., Viti, S., Williams, D. A., 2007b, *MNRAS*, 378, 983
- Bertram, T.; Eckart, A.; Fischer, S.; Zuther, J.; Straubmeier, C.; Wisotzki, L.; Krips, M., 20007, *A&A*, 470, 571
- Brand, K., et al., 2006, 644, 143
- Carilli, C. L.; et al., 2002, *AJ*, 123, 1838
- Condon, J.J., Cotton, W.D., Yin, Q.-F., Shupe, D.L., Storrie-Lombardi, L.J., Helou, G., Soifer, B.T., & Werner, M.W., 2003, *AJ*, 125, 2411
- Condon, J. J., Cotton, W. D., Greisen, E. W., et al. 1998, *AJ*, 115, 1693
- Coppin, K. E. K.; et al., 2008, *MNRAS*, 389, 45
- Cox, P.; et al., 2002, *A&A*, 387, 406
- Daddi, E., et al. 2010, *ApJ*, 713, 686
- Daddi, E., Dannerbauer, H., Krips, M., Walter, F., Dickinson, M., Elbaz, D., & Morrison, G. E. 2009, *ApJ*, 695, L176
- Dale, D.A., & Helou, G., 2002, *ApJ*, 576, 159
- Downes, D., & Solomon, P. M. 1998, *ApJ*, 507, 615
- Evans, A. S.; Frayer, D. T.; Surace, J. A.; Sanders, D. B., 2001, *AJ*, 121, 1893
- Franceschini, A.; et al., 2003, *MNRAS*, 343, 1181
- Feigelson, E.D.; Nelson, P.I., 1985, *ApJ*, 293, 192
- Feruglio, C.; Maiolino, R.; Piconcelli, E.; Menci, N.; Aussel, H.; Lamastra, A.; Fiore, F., 2010, *A&A*, 518, L155
- Frayer, D. T.; et al., 2006, *AJ*, 131, 250
- Gao, Y.; & Solomon, P.M., 2004, *ApJ*, 606, 271
- Greve, T. R.; et al., 2005, *MNRAS*, 359, 1165
- Greve, T. R.; Sommer-Larsen, J., 2008, *A&A*, 480, 335
- Hainline, L. J.; Scoville, N.Z.; Yun, M.S.; Hawkins, D. W.; Frayer, D. T.; Isaak, K. G., 2004, *ApJ*, 609, 61
- Hasinger, G., 2008, *A&A*, 490, 905
- Hopkins, P.F.; Hernquist, L.; Cox, T.J.; Di Matteo, T.; Robertson, B.; Springel, V., 2006, *ApJS*, 163, 1
- Imanishi, M.; Dudley, C. C.; Maiolino, R.; Maloney, P. R.; Nakagawa, T.; Risaliti, G., 2007, *ApJS*, 171, 72
- Iono, D.; Wilson, Ch. D.; Yun, M.S.; Baker, A.J.; Petitpas, G.R.; Peck, A.B.; Krips, M.; Cox, T. J.; Matsushita, S.; Mihos, J. Ch.; Pihlstrom, Y., 2009, *ApJ*, 695, 1537
- Krips, M.; Eckart, A.; Neri, R.; Zuther, J.; Downes, D.; Scharwächter, J., 2005a, *A&A*, 439, 75
- Krips, M., Neri, R., Eckart, A., Downes, D., Martín-Pintado, J., & Planesas, P. 2005b, *A&A*, 431, 879
- Krips, M.; et al., 2007, *A&A*, 464, 187
- Krips, M.; et al., 2011, *ApJ*, 736, 37
- Lacy, M.; et al., 2004, *ApJS*, 154, 166
- Lacy, M.; et al., 2007a, *ApJ*, 669, L61
- Lacy, M.; et al., 2007b, *AJ*, 133, 186
- La Franca, F., et al., 2005, *ApJ*, 635, 864
- Maiolino, R.; et al., 2007, *A&A*, 472, L33
- Martínez-Sansigre, A.; et al., 2006, *MNRAS*, 370, 1479
- Matsushita, S.; et al., 2007, *A&A*, 468, L49
- Narayanan, D.; et al., 2006, *ApJ*, 642, L107
- Narayanan, D.; Cox, Th. J.; Shirley, Y.; Dave, R.; Hernquist, L.; Walker, Ch. K., 2008a, *ApJ*, 684, 996
- Narayanan, D.; et al., 2008b, *ApJS*, 174, 13
- Narayanan, D.; et al., *ApJS*, 176, 331N
- Neri, R., et al. 2003, *ApJ*, 597, L113
- Polletta, M., et al. 2011, *A&A*, 533, A20
- Pott, J.-U.; Eckart, A.; Krips, M.; Tacconi-Garman, L. E.; Lindt, E., *A&A*, 456, 505-508 (2006)
- Reyes, R.; et al., 2008, *ApJ* 136, 2373
- Riechers, D. A., et al. 2009, *ApJ*, 703, 1338
- Riechers, D. A. 2011, *ApJ*, 730, 108
- Sakamoto, K.; Okumura, S.K.; Ishizuki, S.; Scoville, N. Z., 1999, *ApJS*, 124, 403
- Sanders, D.B.; Soifer, B.T.; Elias, J.H.; Neugebauer, G.; Matthews, K., 1988a, *ApJ*, 328, L35
- Sanders, D. B.; Soifer, B. T.; Elias, J. H.; Madore, B. F.; Matthews, K.; Neugebauer, G.; Scoville, N. Z., 1988b, *ApJ*, 325, 74S
- Scoville, N. Z.; Frayer, D. T.; Schinnerer, E.; Christopher, M., 2003, *ApJ*, 585, L105
- Simpson, C., et al., 2006, *MNRAS*, 372, 741
- Solomon, P. M.; Barrett, J. W., 1991, "Dynamics of Galaxies and Their Molecular Cloud Distributions", Proceedings of the 146th Symposium of the International Astronomical Union, held in Paris, France, June 4-9, 1990, ed. by F. Combes and Fabienne Casoli, IAUS No. 146, Kluwer Academic Publishers, Dordrecht, , p.235
- Tacconi, L. J., et al. 2010, *Nature*, 463, 781
- Tacconi, L. J., et al. 2008, *ApJ*, 680, 246
- Tacconi, L. J., et al. 2006, *ApJ*, 640, 228
- Treister, E.; Urry, C. M., 2006, *ApJ*, 652, L79
- Vila-Vilaró, B.; Taniguchi, Y.; Nakai, N., 1998, *AJ*, 116, 1553
- Walter, F.; Carilli, C.; Bertoldi, F.; Menten, K.; Cox, P.; Lo, K. Y.; Fan, X.; Strauss, M. A., 2004, *ApJ*, 615, L17
- Wang, R., et al. 2011, *AJ*, 142, 101
- Wang, R., et al. 2011, *ApJ*, 739, L34
- Wink, J. E.; Guilloteau, S.; Wilson, T. L, 1997, *A&A*, 322, 427
- Zakamska, N.L.; Gómez, L.; Strauss, M. A.; Krolik, J. H., 2008, *AJ*, 136, 1607